Journal of
Synchrotron Radiation

ISSN 0909-0495

Received 8 June 2005
Accepted 23 February 2006

Optimizing the signal-to-noise ratio for X-ray photon correlation spectroscopy

P. Falus,[a]* L. B. Lurio[b] and S. G. J. Mochrie[c]

[a]Institute Laue Langevin, Grenoble F-38042, France, [b]Department of Physics, Northern Illinois University, DeKalb, IL 60115, USA, and [c]Departments of Physics and Applied Physics, Yale University, New Haven, CT 06520, USA. E-mail: falus@ill.fr

An analysis is presented of how to optimize the experimental beamline configuration for achieving the best possible signal-to-noise ratio (SNR) in X-ray photon correlation spectroscopy experiments using area detectors. It is shown that there exists an optimum detector distance; namely, the highest SNR is achieved by matching the angular pixel size with the angular source size. Binning several pixels together can increase the SNR by permitting to match the shape of a detector pixel to the shape of the source. It is also shown that collimating slits several times wider than the effective transverse coherence length are optimal; further, it is demonstrated that the energy dependence of the SNR is dictated by the energy dependence of detector efficiency and source brilliance. Ultimately the effects of focusing and low longitudinal coherence are discussed.

Keywords: photon correlation; XPCS; area detectors; optimum distance; pixel size.

1. Introduction

X-ray photon correlation spectroscopy is an emerging new method that can now be used at high-brilliance synchrotron beamlines for characterizing the dynamics of slowly moving condensed matter (Falus *et al.*, 2005; Sutton *et al.*, 1991; Brauer *et al.*, 1995; Dierker *et al.*, 1995; Thurn-Albrecht *et al.*, 1996; Mochrie *et al.*, 1997; Tsui & Mochrie, 1998; Thurn-Albrecht *et al.*, 1999; Price *et al.*, 1999; Lurio *et al.*, 2000; Lumma, Lurio, Sandy *et al.*, 2000; Lumma *et al.*, 2001; Seydel *et al.*, 2001; Livet *et al.*, 2001; Dufresne *et al.*, 2002; Sikharulidze *et al.*, 2002; Kim *et al.*, 2003; Madsen *et al.*, 2003). Typically, to carry out X-ray photon correlation spectroscopy (XPCS) experiments, the X-ray beam from a high-brilliance X-ray source is monochromated and apertured to a size approximately equal to the transverse coherence length of the source. This creates a partially coherent X-ray beam, which illuminates a sample of interest. Density fluctuations within the sample cause scattering, giving rise to a time-varying X-ray speckle pattern, which is captured moment-by-moment by a detector. The two-time correlation of the intensities in each pixel yields the intensity auto-correlation function, g_2, which shows the characteristic relaxation times of the sample. Specifically, g_2 is related to the sample's intermediate scattering function (ISF), $S(Q, t)$, *via*

$$g_2 = 1 + A[S(Q, t)]^2. \quad (1)$$

where A is the optical contrast, which depends on the parameters of the experimental set-up. At present, XPCS is a signal-limited technique and therefore it is important to optimize as far as possible the signal-to-noise ratio (SNR). Minimizing sample damage also calls for the most efficient use of X-rays. Moreover, there are presently several major proposals to construct new very high brilliance X-ray sources: (NSLS2 Brookhaven, ERL Cornell, MIT-Bates XFEL, LCLS Stanford). High-brilliance experiments, of which XPCS is one important example, provide the scientific rationale for these machines. It is essential to understand the ingredients that allow one to optimize the XPCS SNR in order to make informed decisions concerning the layout and design of beamlines that might be destined for XPCS experiments. In this paper we elaborate calculations (Lumma, Lurio, Mochrie & Sutton, 2000) of the anticipated SNR in XPCS experiments in order to answer the following questions: what is the optimum aperture before the sample for a given source size? Is there an optimum sample-to-detector distance for given CCD pixel dimensions and given number of pixels? Is it possible to improve the SNR by binning together the intensity in spatially separated pixels, and if so how many? How does the SNR change with X-ray energy?

2. Signal-to-noise ratio

We consider a synchrotron beamline that consists of a partially coherent source, a sample, adjustable collimating slits close to the sample, and an area detector (CCD). Throughout this paper we will use the numerical values relevant to beamline 8-ID at the Advanced Photon Source (APS), where our XPCS experiments have been carried out, and also to a hypothetical XPCS beamline at the proposed NSLS-II synchrotron at

Brookhaven National Laboratory. In the case of 8-ID the beam-defining slits are located 65 m from the source and the sample is 1.3 m further downstream of the slits. As long as the sample is in the near field of the slits (in this case if the slits are bigger than 15 μm) there is a negligible difference between the slits size and the beam width at the sample. We denote the horizontal and vertical source size as σ_x and σ_z, respectively. At 8-ID we take $\sigma_x = 220$ μm and $\sigma_z = 15$ μm, while at NSLS-II we use $\sigma_x = 54.5$ μm and $\sigma_z = 3.9$ μm. These are the standard deviations of an assumed Gaussian profile for the source intensity, so that the full width at half-maximum of the source intensity is $(8\ln 2)^{1/2}\sigma \simeq 2.35\sigma$. At 8-ID the source-to-sample distance is $R' = 65$ m. For a hypothetical beamline at NSLS-II, we assume $R' = 32$ m, simply scaling the source-to-sample distance by the size of the ring. The angular source sizes are defined as $\theta_z = (8\ln 2)^{1/2}\sigma_z/R'$, $\theta_x = (8\ln 2)^{1/2}\sigma_x/R'$. The transverse coherence length (Sandy *et al.*, 1999) is defined as

$$\xi_x = \frac{\lambda R'}{2\pi\sigma_x} = \frac{(8\ln 2)^{1/2}}{2\pi}\frac{\lambda}{\theta_x}, \tag{2}$$

where $\lambda = 0.185$ nm is the X-ray wavelength. The CCD detector consists of pixels of linear size U_x by U_z, and we define the angular size of pixels as $\omega_x = U_x/R_{\rm det}$ and $\omega_z = U_z/R_{\rm det}$, where $R_{\rm det}$ is the slit-to-detector distance. Using these parameters it may be shown (Lumma, Lurio, Mochrie & Sutton, 2000; Sandy *et al.*, 1999) that we can introduce the *effective* transverse coherence length in the horizontal direction as

$$\begin{aligned}\Xi_x &= \frac{\xi_x}{\left[1 + (U_x^2 R'^2)/\left(8\ln 2\,\sigma_x^2 R_{\rm det}^2\right)\right]^{1/2}} \\ &= \frac{(8\ln 2)^{1/2}\,\lambda}{2\pi}\frac{1}{(\omega_x^2 + \theta_x^2)^{1/2}}.\end{aligned} \tag{3}$$

Analogously defined is Ξ_z, which is the effective coherence length in the z-direction. The effective coherence lengths fold the non-zero detector resolution into the source size (Abernathy *et al.*, 1998). The longitudinal coherence length is given by

$$\Lambda \simeq \lambda(E/\Delta E). \tag{4}$$

For the germanium [111] monochromator currently used at 8-ID, the relative bandwidth is almost energy independent with $E/\Delta E \simeq 3 \times 10^3$. In a small-angle-scattering geometry, the longitudinal coherence length will only effect the speckle contrast when it becomes comparable with the maximum pathlength difference in the sample, δ, which is given by

$$\begin{aligned}\delta = {} & 2\sin\psi\cos\psi\cos\varphi\, L_x + 2\sin\psi\cos\psi\sin\varphi\, L_z \\ & + 2\sin^2\psi\, W,\end{aligned} \tag{5}$$

where L_x, L_z and W are the dimensions of the scattering volume in the horizontal, vertical and along-the-beam directions, respectively, ψ is the scattering angle and φ is the azimuthal angle from the horizontal scattering plane. The contrast is reduced by a finite longitudinal coherence length by a factor of approximately

$$\exp(-|\delta|/\Lambda). \tag{6}$$

Typically, at 8-ID, we have $L_x = L_z = 50$ μm, while the sample thickness, W, is comparable with the absorption length which depends on the sample material and energy. For a typical hydrocarbon studied using 6.7 keV X-rays the attenuation length (and consequently a typical sample thickness) is $\sim$1.6 mm. Choosing $Q = 0.2$ nm^{-1} gives $\delta/\Lambda \simeq 0.1$, resulting in a less than 10% correction to the contrast for the typical case of $Q < 0.2$ nm^{-1}. The effects of a finite longitudinal coherence length will be discussed in more detail in §6.

Further, following the calculation of Lumma, Lurio, Mochrie & Sutton (2000) and ignoring, for now, the effects of longitudinal coherence we can write the optical contrast (A) of the speckle patterns as

$$A = F(L_x/\Xi_x)F\left(L_z/\Xi_z\right), \tag{7}$$

where L_x and L_z denote the horizontal and vertical slit widths, respectively, and F is the contrast function, given by

$$F(x) = \left(1/x^2\right)\left[x\,\pi^{1/2}\,\mathrm{erf}(x) + \exp\left(-x^2\right) - 1\right], \tag{8}$$

where erf(...) is the error function. It will be useful to note that, for $x \gg 1$, $F(x) \simeq \pi^{1/2}/x$, and that, for $x \ll 1$, $F(x) \simeq 1 - x^2/6$.

In considering the SNR, the low-count-rate limit is the appropriate limit for XPCS. Jakeman has shown that, in this limit, the variance of g_2 is given by

$$\mathrm{var}\, g_2 = g_2/\left(M\bar{n}^2\right), \tag{9}$$

where $\bar{n}$ is the mean number of counts detected per accumulation time and M is the total number of correlated pairs averaged to yield g_2 (Jakeman, 1973). This may be re-written in terms of the count rate ($\bar{I}$) per CCD pixel, the accumulation time (τ), the number of pixels ($n_x \times n_z$) and the total experimental duration (T) as

$$\mathrm{var}\, g_2 = g_2/\left(n_x n_z T\tau\bar{I}^2\right). \tag{10}$$

A sensible measure of the SNR is

$$R_{\rm sn} = (g_2 - 1)/(\mathrm{var}\, g_2)^{1/2} = \left(T\tau\, n_x n_z/g_2\right)^{1/2}\,\bar{I}(g_2 - 1). \tag{11}$$

A simplified expression, suitable for comparing different experimental parameters, is obtained by combining (10) and (11), substituting g_2 with its zero time limit $1 + A$, and assuming that $g_2^{1/2} \simeq 1$, *i.e.* that the contrast is small,

$$R_{\rm sn} = A\bar{I}\left(T\tau\, n_x n_z\right)^{1/2}. \tag{12}$$

In fact, we define (12) to be the SNR in XPCS experiments and seek to maximize it. Equation (12) shows that for XPCS the SNR is linearly proportional to the scattering intensity, in contrast to ordinary intensity measurements where the SNR is proportional to the square root of the intensity. On the other hand, the XPCS SNR is proportional to the square root of the experimental duration (T), just as for scattering experiments.

In an XPCS experiment the goal is to measure $g_2(Q, t)$ (and thus the ISF) as a function of time (t) and wavevector (Q). With an area detector it is possible to acquire data at many

different wavevectors simultaneously. However, data with insufficient SNR at many different values of Q are worthless. It follows that in assessing the consequences of (12) we should focus on the SNR for a particular value of Q within some desired Q-resolution, not the whole area of the detector. In the context of an experiment, this corresponds to the scattered X-rays that fall within a definite solid-angular range of particular scattering angles. Thus, in (12), the values of n_x and n_y correspond to this solid angular range. It is therefore convenient to introduce the angle subtended by the Q of interest in the x-direction (Ω_x) and in the z-direction (Ω_z). In terms of the angular extent of each pixel, ω_x and ω_z in the x- and z-directions, respectively, and Ω_x and Ω_z, we may express the number of pixels appearing in (12) as $n_x = \Omega_x/\omega_x$ and $n_z = \Omega_z/\omega_z$. In this paper we will usually assume that n_x and n_z do not exceed the number of rows and columns available on the detector (or detectors).

The count rate per pixel ($\bar{I}$) depends on the incident flux density (Φ), the solid angle subtended by each pixel, the scattering cross section per unit volume of the sample (Σ), the detector efficiency (K), the illuminated sample area ($L_x \times L_z$) and the sample thickness (W) and attenuation length (Λ) *via*

$$\bar{I} = K\Phi L_x L_z \omega_x \omega_z \Sigma W \exp(-W/\Lambda). \tag{13}$$

[Equation (13) assumes that the flux is constant over the illuminated sample area.] The flux density, in turn, can be expressed in terms of the source brilliance $\tilde{B}$, the relative energy bandwidth $\Delta E/E$ and the angular source sizes, yielding

$$\Phi = \tilde{B}(\Delta E/E)[2\pi/(8\ln 2)]\,\theta_x\theta_z. \tag{14}$$

Using (2), (7), (12), (13) and (14) we obtain

$$R_{\rm sn} = K\left(T\tau\,\Omega_x\Omega_z\right)^{1/2}\Sigma W \exp(-W/\Lambda)\tilde{B}(\Delta E/E) r_{{\rm sn}x} r_{{\rm sn}z}, \tag{15}$$

where $r_{{\rm sn}x}$ depends solely on the horizontal pixel size, the horizontal source size and the horizontal slit size. Similarly, $r_{{\rm sn}z}$ depends solely on the vertical parameters. Specifically,

$$r_{{\rm sn}x} = F(L_x/\Xi_x)\,\omega_x^{1/2}\,\theta_x L_x, \tag{16}$$

with an analogous expression for $r_{{\rm sn}z}$. The factorization of (15) permits us to optimize the SNR separately for the vertical and the horizontal directions. Equation (15) further informs us that the SNR is linearly proportional to the source brilliance, but proportional to the square root of the accumulation time (τ). This scaling is especially interesting in the context of proposals for more-brilliant X-ray sources. It implies that, for a sample with a given scattering cross section, if one increases the source brilliance by a factor f then one may decrease the accumulation time by a factor of $f^{1/2}$ to achieve the same SNR. For example, with a 100-fold increase in $\tilde{B}$, one may keep the total measurement time constant, and reduce the shortest correlation time τ by $(100)^2$ to achieve an unchanged SNR. For the present, (15) also reflects the important facts that the SNR is linearly proportional to the detector efficiency and the sample scattering strength. The SNR is also proportional to $W\exp(-W/\Lambda)$, which is maximized by choosing the sample thickness to be equal to the attenuation length.

3. Optimizing the angular pixel size

In this section we explore whether there is an optimal angular pixel size and whether we can improve the SNR by binning several pixels together or by changing the detector-to-sample distance. In these calculations we will consider the source sizes and the slit sizes to be constant. Our single degree of freedom will be the angular pixel size. As we noted in the previous section, we can optimize the SNR separately for the horizontal and vertical direction. Thus, we seek to optimize (16).

Fig. 1 plots (16) as a function of ω for several slit sizes. It is apparent from this graph that for large slits ($L \gg \xi$) $r_{\rm sn}$ is independent of L. We explore this case first.

3.1. Large slit sizes

For large values of x, $F(x) \simeq \pi^{1/2}/x$. This allows us to simplify (16) to become

$$r_{\rm sn} = \left(\frac{2\ln 2\,\lambda^2}{\pi}\right)^{1/2}\left[\frac{1}{\theta(\theta/\omega + \omega/\theta)}\right]^{1/2}. \tag{17}$$

This informs us first that for large slit sizes the SNR is independent of slit size. The second notable feature is that $r_{\rm sn}$ exhibits a peak at $\omega = \theta$, so that there indeed exists an optimum detector distance for a given pixel size, or *vice versa*. Usually CCD pixel sizes are between 10 and 30 μm; it follows that it may be difficult to achieve the optimum sample-to-detector distance. For example, the optimum sample-to-detector distance for a CCD camera at 8-ID with 14 μm pixels is 24.8 m, dictated by the excellent vertical coherence at the APS. On the other hand the maximum possible sample-to-detector distance in the 8-ID endstation hutch is 7 m. Clearly the SNR of XPCS can only be improved if adequate higher-

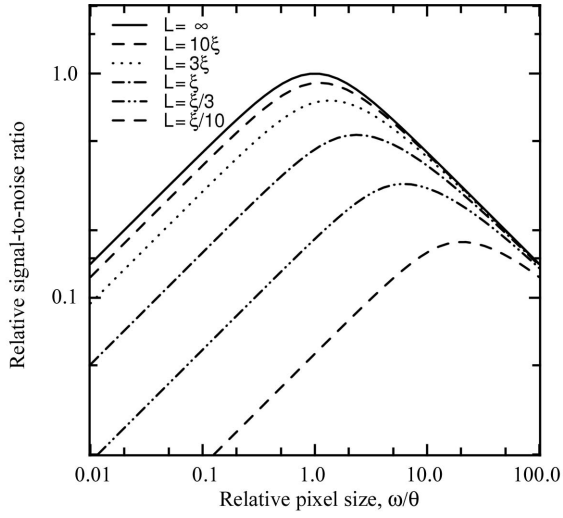

Figure 1
SNR *versus* the ratio of the angular pixel size (ω) and the angular source size (θ) at different slit sizes (L).

resolution detectors are developed. Although the most pressing problem of CCD area detectors is speed (Falus *et al.*, 2004), the SNR can only be optimized if the size of the detector pixels is much smaller then the present sizes. Hopefully, parallel to developing new X-ray sources, new high-efficiency detectors are also being developed.

We should emphasize that Fig. 1 is not valid for point detectors. When we have a single pixel, the detector size $\Omega_z\Omega_x$ is not constant [unlike in (15)]; it scales with the pixel size $\omega_x\omega_z$. Then Fig. 1 is modified such that for large pixel sizes the SNR is constant; for small ω the SNR will decay linearly with ω. Thus we will have a lower limit on pixel size, but no higher limit. The SNR is optimal for point detectors as long as the detector size is bigger than the speckle size.

It is also interesting to note that to achieve the maximum SNR requires pixels with an aspect ratio that is the same as the aspect ratio of the source. For the usual case of cameras with square pixels, this can be achieved by binning or adding the signal from several pixels in the horizontal direction. These considerations suggest that the optimum experimental set-up at 8-ID would be achieved by moving the camera as far back as possible in the hutch, so as to approach as closely as possible the condition $\omega_z = \theta_z$. At this distance, ω_x will be smaller than θ_x but this can be compensated by binning several pixels together until $\omega_x = \theta_x$.

To elucidate how important is it to achieve these optimum conditions, it is useful to employ the approximation that $r_{sn} \simeq r_{sn_{max}}(2\omega/\theta)^{1/2}$, which is approximately valid for $\theta/\omega > 3$. Then we may examine the following three 8-ID-based examples:

(i) Using a camera with 14 μm × 14 μm pixels at 1.7 m from the sample, the horizontal size is optimal, the vertical size is larger than optimal by a factor of 14 causing the SNR to be $7^{1/2} = 2.6$ smaller than optimal. This is a significant loss of SNR from that optimally possible.

(ii) Using the same camera with 14 μm × 14 μm pixels at 7 m, the vertical pixel size is a factor of 3.5 larger than optimal, while the horizontal pixel size is a factor of four smaller than optimal. It follows that the SNR is $[(3.5/2)(4/2)]^{1/2} \simeq 1.9$ less than optimal. This too represents an important loss of SNR.

(iii) Using the same camera with 14 μm × 14 μm pixels at 7 m but now binning four pixels horizontally, the vertical pixel size is a factor of three larger than optimal, while the effective horizontal pixel size (56 μm) is optimal. In this case the SNR is $(3.5/2)^{1/2} = 1.3$ times smaller than optimal, which is a considerably better situation than in (i) and (ii).

These considerations are modified in the case where the detector area is not large enough to accept all of the scattering at the wavevector of interest. This is not a fundamental issue, since in principle we may tile together a number of smaller detectors to make an arbitrarily large detector, which would be able to accept all of the scattering at a given wavevector. Nevertheless, for a single detector the finite detector acceptance is of practical relevance. In particular, for isotropic systems, which give rise to circularly symmetric rings of scattering, we can average g_2 from all the pixels within rings that correspond to the same wavenumber. If the detector acceptance is not large enough to detect the entire ring, the detected solid angle is reduced by a factor proportional to R^{-1}. Consequently, for high wavenumbers the number of pixels in the ring varies as R_{det}, not as R_{det}^2, resulting in a $R_{det}^{-1/2}$ correction to our calculation or the SNR.

Again taking into account the scaling form of $r_{sn} \propto R_{det}^{1/2}$ for $\omega \gg \theta$, and $r_{sn} \propto R_{det}^{-1/2}$ for $\omega \ll \theta$ (large R_{det}), noting that the azimuthal correction varies as $R_{det}^{-1/2}$, and noting that in case of optimum binning r_{sn} is constant for $\omega < \theta$, we distinguish four cases which are demonstrated in Fig. 2:

(i) The detector intercepts all of the scattering, but we do not use binning. The SNR has a wide peak between the $\omega_x = \theta_x$ and $\omega_z = \theta_z$ points. With 8-ID parameters the peak is between $R_{det} = R_x = 1.7$ m and $R_{det} = R_z = 25$ m. This case is shown by curve '$Q = 0$' in Fig. 2.

(ii) The detector intercepts all of the scattering and we use optimal binning. As shown in curve '$Q = 0$ bin' in Fig. 2, the SNR will increase with increasing sample-to-detector distance until we have moved the detector as far as R_z. Beyond R_z, the SNR remains approximately constant (the discernible dips in the theoretical SNR from twofold to threefold binning and from threefold to fourfold binning *etc.*).

(iii) The detector does not intercept all of the ring of scattering of interest and we do not use binning. Here the SNR peaks at a detector distance of R_x and decreases sharply for larger sample-to-detector distances, as shown by curve '$Q = 0.2$ nm^{-1}'.

(iv) The detector does not intercept all of the ring of scattering and we use optimal binning. In this case the SNR shows a broad maximum for sample-to-detector distances between R_x and R_z, and we have a wide range within which to set the sample-to-detector distance (see curve '$Q = 0.2$ nm^{-1} bin' in Fig. 2).

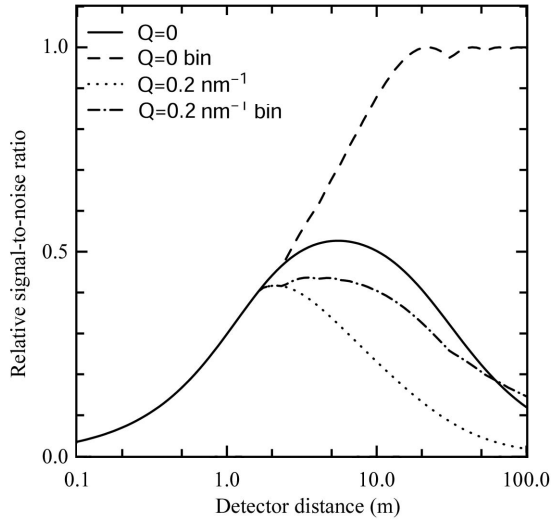

Figure 2
SNR *versus* sample-to-detector distance, calculated with parameters appropriate to 8-ID. Specifically, the detector pixel size is 14 μm, the source size is 220 μm × 15 μm, the slit size is 1000 μm and the photon energy is 6.7 keV. For reference, with these parameters $\theta_x = \omega_x$ occurs at a distance of 1.7 m, $\theta_z = \omega_z$ at 25 m. The wiggles on the binned curves are the result of taking the maximum of several peaks corresponding to all possible binnings.

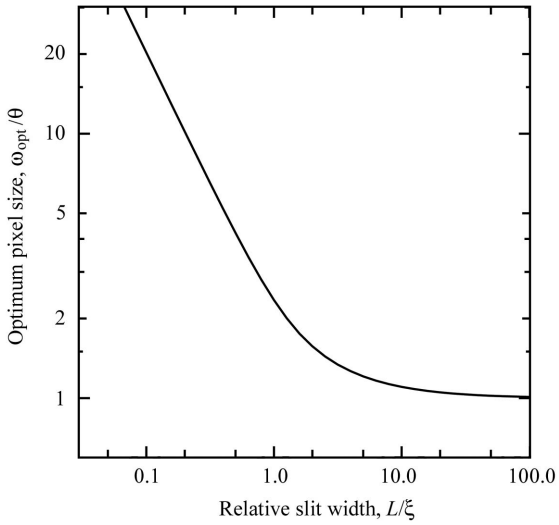

Figure 3
Ratio of the angular pixel size ω and the angular source size θ at maximum signal-to-noise ratio *versus* slit size. The optimum values are deduced by numerically finding the maximum of curves similar to the ones in Fig. 1.

3.2. Small slit sizes

It is clear from Fig. 1 that, for slit sizes smaller than about three coherence lengths, the SNR displays a significant L dependence. In fact, the maximum SNR decreases with decreasing L, while the optimum pixel acceptance ω increases with decreasing L. This is highlighted in Fig. 3, which plots *versus* L the values of ω at which the SNR is a maximum for a particular L.

An analytically tractable expression for the L-dependence of the maximum SNR follows from the approximation that $F(x) \simeq 1 - x^2/6$, which is valid for $L/\Xi \ll 1$. The location of the maximum SNR in this limit is

$$\omega_{\rm opt} = (12 \ln 2)^{1/2} \lambda / \left(5^{1/2} \pi L\right) \simeq 0.41 \lambda / L, \qquad (18)$$

which varies inversely with the slit width and, interestingly, is independent of the angular source size. Careful inspection of the curve in Fig. 3 for $L/\xi \ll 1$ reveals an $\omega_{\rm opt} \simeq 0.78\lambda/L$ dependence. Thus, the first-order analytical approximation is not precise enough to find the exact maximum; the scaling is preserved though. This limit is especially important in the case of X-ray free-electron lasers, where the fully coherent beam corresponds to $\theta = 0$ and the optimum pixel size will always be determined by the beam size (speckle size).

4. Determining the best slit size

As already noted, for large slits the SNR is independent of slit size, while for small slits the SNR decreases linearly with the slit size. In this section we will explore the dependence of the SNR on the slit size for constant pixel size (ω) and constant source size (θ). Since we know that the maximum SNR is achieved in the large-slit limit [equation (17)] for any ω, it is instructive to plot the ratio

Table 1
SNR and contrast for several slit settings at 8-ID.

Slit width	Slit height	Contrast	SNR relative to maximum
$2\Xi_x$	$2\Xi_z$	0.40	0.52
$4\Xi_x$	$4\Xi_z$	0.14	0.74
$6\Xi_x$	$6\Xi_z$	0.07	0.82
$11\Xi_x$	$3\Xi_z$	0.07	0.77

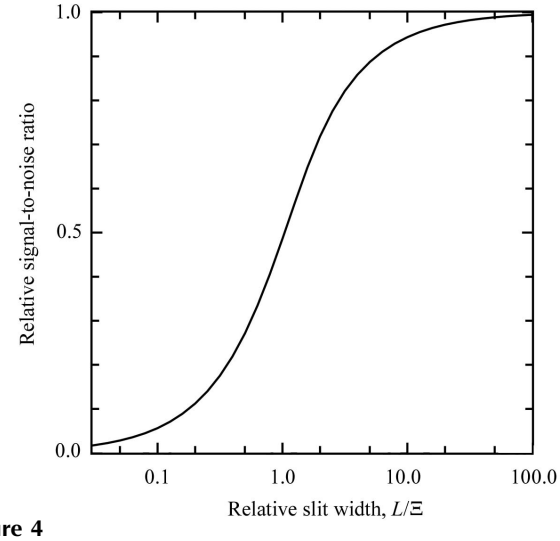

Figure 4
Relative SNR *versus* slit size while keeping θ and ω fixed

$$\frac{r_{\rm sn}(L)}{r_{\rm sn}(\infty)} = F\left(\frac{L}{\Xi}\right) \frac{1}{\pi^{1/2}} \frac{L}{\Xi}. \qquad (19)$$

This function depends only on L/Ξ. It is apparent from Fig. 4 that the SNR increases monotonically with L, reaching 0.5 for $L/\Xi = 1$, 0.8 for $L/\Xi = 3$, and 0.9 for $L/\Xi = 6$. This confirms that, while widening the slits is generally beneficial, opening them too much past a few times the effective coherence length will not significantly increase the SNR. It is not surprising either that, for $L/\Xi \ll 1$, $r_{\rm sn}$ is proportional to L, since in this case closing the slits does not increase the contrast but merely reduces the intensity.

If L/Ξ is very large, the optical contrast is correspondingly very small, and it may be preferable to instead maintain a certain level of contrast in order to insure against any systematic errors that might create small baseline shifts. Some examples are given in Table 1.

As a compromise between the best SNR and non-zero contrast, it is sensible to set the slit width to be several times (three to six times) wider than the coherence length, which will yield contrast values between 0.07 and 0.14. It is also clear from the last two lines that, while setting the slit width symmetrically produces the best SNR, asymmetric set-ups yield a SNR that is only slightly lower.

5. Optimizing energy

Since the efficiency of direct-detection CCD detectors is invariably X-ray energy dependent, and since at 8-ID and other beamlines one generally has considerable freedom in

choosing at what energy to carry out an XPCS experiment, it is valuable to investigate the effects of varying the X-ray energy on the SNR. We first consider how to optimize the energy in the limit of large slits. We furthermore suppose that when we tune the energy we keep fixed the range of wavevectors contributing to the particular Q of interest. It follows that $\Omega_x\Omega_z$ must be varied to maintain this range of wavevectors, while ω and θ are fixed (and optimally equal to each other). In addition, we suppose that we adjust the sample thickness (W) in order to keep the sample attenuation constant, *i.e.* we set $W = \Lambda(E)$. Equation (17) then informs us that $r_{snx}r_{snz}$ varies as E^{-2} because of the factor λ^2. Other energy-dependent factors in (15) are $(\Omega_x\Omega_z)^{1/2}$, which is proportional to E^{-1}, and $W\exp(-W/\Lambda)$, which is material-dependent but is often proportional to E^3. Thus, to leading order, these factors cancel each other out. The remaining factors are the source brilliance and the detector efficiency. In addition, at 8-ID we should recognize that there is an energy-dependent attenuation owing to Be windows in the beamline. For the APS, the brilliance varies weakly with energy with a peak at about 7 keV. Reducing the X-ray energy can significantly increase the CCD detector's quantum efficiency (at least within the range 4–10 keV) and can reduce the spreading of photons (Hashimotodani, 1998). In its simplest form the CCD detector efficiency varies as $\eta = 1 - \exp(-d_{dep}/\Lambda_{Si})$ where d_{dep} is the depletion layer thickness, and the silicon attenuation length $\Lambda_{Si} \propto E^3$, strongly favoring low energies. Both of these effects tend to improve the SNR at lower energies. By contrast, the attenuation of Be windows increases sharply for energies below about 5 keV. Thus, for 8-ID or other beamlines in which there are Be windows, we expect that the optimum X-ray energy for XPCS is about 6 keV (see Fig. 5). Since Be windows are far from perfect optics, it would be desirable in any case to find an improved X-ray window material. With a different window material the calculus leading to the prediction that the SNR will be optimal at 6 keV will be changed somewhat. In the case of a sample with isotropic scattering, so that at high wavenumbers the scattering ring does not completely fit on the CCD, an extra factor in the SNR proportional to $E^{1/2}$ becomes necessary. However, this moves the optimum energy only slightly. While in Fig. 5 the longitudinal and azimuthal correction was calculated for all wavenumbers, neither of the corrections have an effect on the solid line, and the dashed line is only affected by the azimuthal correction. For anisotropic systems at wavenumbers where the longitudinal correction is negligible, the solid line should be used.

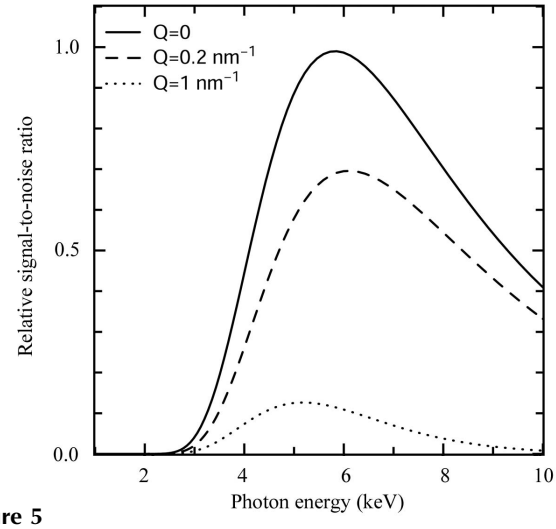

Figure 5
Energy dependence of the SNR for parameters relevant to 8-ID. The brilliance of the APS undulator A, the attenuation of four 0.25 mm Be windows, and the measured efficiency and detector size of the SMD 1M60 detector (Falus *et al.*, 2004) are taken into account. The SNR is calculated taking into account the effect of longitudinal coherence and the correction for azimuthal averaging. The solid line is unaffected both by the longitudinal and azimuthal correction.

Our conclusions are different from those of Thurn-Albrecht *et al.* (2003), who predict that the SNR in an XPCS experiment has an overall E^2 dependence. The chief points of difference between our analysis and that of Thurn-Albrecht *et al.* involve the factors dealing with the efficiency of a CCD camera, the angular factor of $(\Omega_x\Omega_z)^{1/2}$, and the assumption, made by those authors, that the total measurement time is limited by the rate of sample damage. The first two differences result from the choice of detector: an area detector in the present case and a point detector by Thurn-Albrecht *et al.* In this context we note that a current state-of-the-art area detector yields a much superior SNR than a point detector for correlation times greater than 2 ms (Falus *et al.*, 2004). With regard to the sample damage issue, we assume that the time required to damage the sample is at least a few times longer than the relevant correlation times. Consequently, using an area detector, the sample can be periodically moved to illuminate a fresh spot, so that there is no limitation on overall measurement time (Lumma, Lurio, Mochrie & Sutton, 2000).

6. Longitudinal coherence

The preceding discussion of energy optimization has been made under the assumption that the longitudinal coherence length (Λ) is large in comparison with the maximum optical pathlength difference (δ) within the sample. A detailed calculation of the effect of longitudinal coherence on the contrast requires an integral of the relevant sample volume and energy distributions (Sandy *et al.*, 1999) and is beyond the scope of this paper. In brief, however, with the approximation that the X-ray power spectrum is a Lorentzian, and that the dimensions of the sample transverse to the beam are sufficiently small, then the X-ray contrast will vary as $\exp(-|\delta|/\Lambda)$. If the sample thickness is adjusted to match the attenuation length, then δ will depend on both the energy and wavevector of the measurement. Specifically, in the range of wavevectors where the sample thickness is much bigger than the beam size, equation (5) may be approximated as

$$\delta = W\lambda^2Q^2/8\pi^2. \qquad (20)$$

The energy dependence of (20) results from the factor of λ^2 and the E^3 dependence of the attenuation length. Consequently, since Λ varies as E^{-1}, the ratio δ/Λ will vary as Q^2E^2. Based on this observation, we note that for a scattering wavevector of 0.5 nm^{-1}, for example, it is only sensible to

increase the sample thickness to match the attenuation length of the sample (for typical organic-based materials) out to about 11 keV. At 1 nm^{-1} the effect is so strong that it influences the optimum energy calculation (see Fig. 5).

7. Focusing

So far we have not considered the possibility of focusing in this paper. Since the vertical coherence lengths at synchrotron sources are much greater than the horizontal coherence lengths, it is first sensible to examine the effect of vertical focusing on the coherence properties of the beam. To this end we consider a focusing optic a distance R_1 from the source that focuses to an image at an additional distance R_2 downstream. The image, which is of size $\sigma_z' = R_2\sigma_z/R_1$, may be viewed as a new source, so that the coherence length at the sample position, which we take to be a further distance R_3 downstream, is $\zeta_F = \lambda R_3/2\pi\sigma_z' = \lambda R_3R_1/2\pi\sigma_z R_2$. This may be compared with the coherence length at the sample position in the absence of the focusing optic, which is $\zeta = \lambda(R_1 + R_2 + R_3)/2\pi\sigma_z$, since $R_1 + R_2 + R_3$ is the source-to-sample position. Although the value of R_1 may be constrained by the location of the beamline's first optics enclosure, there remains considerable freedom in the choice of the ratio $\zeta/\zeta_F = (R_1 + R_2 + R_3)R_2/(R_3R_1)$. At 8-ID-I, in particular, it might be convenient to pick $\zeta/\zeta_F = 5$, so that the optimum sample-to-detector distance would become 5 m, which would then lie within the 8-ID-I hutch. This could be arranged, for example, with $R_1 = 35$ m, $R_2 = 22$ m and $R_3 = 8$ m, or with $R_1 = 55$ m, $R_2 = 8$ m and $R_3 = 2$ m. A similar focusing at NSLS-II would reduce the optimum sample-to-detector distance there from 50 m to a more manageable 10 m.

8. Conclusion

In this paper we have explored how to optimize the signal-to-noise ratio in an X-ray photon correlation spectroscopy experiment by revisiting and analyzing the calculation of the optical contrast at a synchrotron source. We demonstrated that for fixed slit size the signal-to-noise ratio for data at a particular wavevector exhibits a maximum *versus* the angular pixel size. For slits wider than the transverse coherence length, we showed that the optimum signal-to-noise ratio is achieved when the angular source size and the angular pixel size are equal to each other. We quantified the well known fact that opening up the collimating slits increases the signal-to-noise ratio but that, once the slit size is larger than several times the effective coherence length, the signal-to-noise ratio does not improve significantly by further increasing the slit size. Finally, we showed that the signal-to-noise ratio depends on the energy mainly through the detector efficiency and window attenuation. Thus, it is sensible to select the X-ray energy accordingly to take advantage of higher detector efficiencies.

In summary, the best signal-to-noise ratio can be achieved by moving the detector sufficiently far back from the sample so that the vertical angular source size is the same as the angular detector pixel size, or, at 8-ID, as far back as possible within the hutch. Then, since the horizontal source size is usually much larger than the vertical source size, we have shown that one should bin together the counts in pixels in the horizontal direction so as to match the effective horizontal pixel size with the horizontal source size.

We thank Matthew Borthwick, Dirk Lumma, Mark Sutton and Brian Stephenson for valuable discussions. This work was supported by the NSF *via* Grant DMR 0453856.

References

Abernathy, D. L., Grübel, G., Brauer, S., McNulty, I., Stephenson, G. B., Mochrie, S. G. J., Sandy, A. R., Mulders, N. & Sutton, M. (1998). *J. Synchrotron Rad.* **5**, 37–47.

Brauer, S., Stephenson, G. B., Sutton, M., Brüning, R., Dufresne, E., Mochrie, S. G. J., Grübel, G., Als-Nielsen, J. & Abernathy, D. L. (1995). *Phys. Rev. Lett.* **74**, 2010.

Dierker, S. B., Pindak, R., Fleming, R. M., Robinson, I. K. & Berman, L. E. (1995). *Phys. Rev. Lett.* **75**, 449–452.

Dufresne, E. M., Nurushev, T., Clarke, R. & Dierker, S. B. (2002). *Phys. Rev. E*, **65**, 061507.

Falus, P., Borthwick, M. A. & Mochrie, S. G. J. (2004). *Rev. Sci. Instrum.* **75**, 4383–4400.

Falus, P., Borthwick, M. A. & Mochrie, S. G. J. (2005). *Phys. Rev. Lett.* **94**, 016105.

Hashimotodani, K. (1998). *Rev. Sci. Instrum.* **69**, 3746–3750.

Jakeman, E. (1973). *Photon Correlation and Light Beating Spectroscopy*, edited by H. Z. Cummins and E. R. Pike, pp. 75–149. New York: Plenum.

Kim, H. J., Ruehm, A., Lurio, L. B., Basu, J., Lal, J., Lumma, D., Mochrie, S. G. J. & Sinha, S. K. (2003). *Phys. Rev. Lett.* **90**, 068302.

Livet, F., Bley, F., Caudron, R., Geissler, E., Abernathy, D., Detlefs, C., Grubel, G. & Sutton, M. (2001). *Phys. Rev. E*, **63**, 036108.

Lumma, D., Borthwick, M. A., Falus, P., Lurio, L. B. & Mochrie, S. G. J. (2001). *Phys. Rev. Lett.* **86**, 2042.

Lumma, D., Lurio, L. B., Mochrie, S. G. J. & Sutton, M. (2000). *Rev. Sci. Instrum.* **71**, 3274.

Lumma, D., Lurio, L. B., Sandy, A. R., Borthwick, M., Falus, P., Mochrie, S. G. J., Sutton, M. & Regan, L. (2000). *Phys. Rev. E*, **62**, 8258.

Lurio, L. B., Lumma, D., Falus, P., Borthwick, M. A., Mochrie, S. G. J., Pelletier, J.-F., Sutton, M., Malik, A. & Stephenson, G. B. (2000). *Phys. Rev. Lett.* **84**, 785.

Madsen, A., Als-Nielsen, J. & Grübel, G. (2003). *Phys. Rev. Lett.* **90**, 085701.

Mochrie, S. G. J., Mayes, A. M., Sandy, A. R., Sutton, M., Brauer, S., Stephenson, G. B., Abernathy, D. L. & Grübel, G. (1997). *Phys. Rev. Lett.* **78**, 1275.

Price, A. C., Sorensen, L. B., Kevan, S. D., Toner, J., Poniewierski, A. & Holyst, R. (1999). *Phys. Rev. Lett.* **82**, 755.

Sandy, A. R., Lurio, L. B., Mochrie, S. G. J., Malik, A., Stephenson, G. B., Pelletier, J.-F. & Sutton, M. (1999). *J. Synchrotron Rad.* **6**, 1174.

Seydel, T., Madsen, A., Tolan, M., Grubel, G. & Press, W. (2001). *Phys. Rev. B*, **63**, 073409.

Sikharulidze, I., Dolbnya, I. P., Fera, A., Madsen, A., Ostrovskii, B. I. & de Jeu, W. H. (2002). *Phys. Rev. Lett.* **88**, 115503.

Sutton, M., Mochrie, S. G. J., Greytak, T., Nagler, S. E., Berman, L. E., Held, G. A. & Stephenson, G. B. (1991). *Nature (London)*, **352**, 608.

Thurn-Albrecht, T., Grübel, G., Müller-Buschbaum, W. S. P. & Patkowski, A. (2003). *Phys. Rev. E*, **68**, 031407.

Thurn-Albrecht, T., Meier, G., Müller-Buschbaum, P., Patkowski, A., Steffen, W., Grübel, G., Abernathy, D. L., Diat, O., Winter, M., Koch, M. G. & Reetz, M. T. (1999). *Phys. Rev. E*, **59**, 642–649.

Thurn-Albrecht, T., Steffen, W., Patkowski, A., Meier, G., Fisher, E. W., Grübel, G. & Abernathy, D. L. (1996). *Phys. Rev. Lett.* **77**, 5437–5440.

Tsui, O. K. C. & Mochrie, S. G. J. (1998). *Phys. Rev. E*, **57**, 2030.